THE LIGHT CURVE OF THE UNUSUAL SUPERNOVA 2003DH

S. E. Woosley

Department of Astronomy and Astrophysics, University of California, Santa Cruz, CA 95064

`woosley@ucolick.org`

and

A. Heger

Theoretical Astrophysics Group, T-6, MS B227, Los Alamos Nation Laboratory, Los Alamos, NM 87545, and
Enrico Fermi Institute, University of Chicago, 5640 S. Ellis Ave., Chicago, IL 60637

`1@2sn.org`

ABSTRACT

SN 2003dh, one of the most luminous supernovae ever recorded, and the one with the highest measured velocities, accompanied gamma-ray burst 030329. Its rapid rise to maximum and equally rapid decline pose problems for any spherically symmetric model. We model the supernova here as a very energetic, polar explosion that left the equatorial portions of the star almost intact. The total progenitor mass was much greater than the mass of high-velocity ejecta, and the total mass of ^{56}Ni synthesized was about 0.5 solar masses. Such asymmetries and nickel masses are expected in the collapsar model. A "composite two-dimensional" model is calculated that agrees well with the characteristics of the observed light curve. The mass of ^{56}Ni required for this light curve is $0.55\,\mathrm{M}_\odot$ and the total explosion energy, 26×10^{51} erg.

Subject headings: gamma rays: bursts; supernovae

1. INTRODUCTION

On March 29, 2003 one of the brightest gamma-ray bursts (GRBs) in history was discovered and localized by the HETE-2 satellite. Astronomers worldwide watched and within days were rewarded by the discovery of a Type Ic supernova, SN 2003dh, in precisely the same location (Stanek et al. 2003; Hjorth et al. 2003). From the light curve and spectrum, a temporal coincidence with the burst was also estimated to be $\lesssim 2$ days. It is now generally agreed that the supernova and the GRB came from the same explosion.

The V-band light curve and spectrum of SN 2003dh closely resembled that of another famous supernova-GRB pair, SN 1998bw (Galama et al. 1998) and GRB 980425, but with several important distinctions: **1)** GRB 980425 had an observed equivalent isotropic energy in gamma-rays roughly four orders of magnitude less than GRB 030329; **2)** SN 2003dh rose to maximum in less than 10 days, SN 1998bw took 16 days (Woosley, Eastman, & Schmidt 1999); **3)** SN 2003dh exhibited higher expansion speeds, up to $40,000\,\mathrm{km\,s^{-1}}$; and **4)** the total energy of ejected relativistic matter in SN 1998bw was $\lesssim 3\times10^{50}$ with $v > 0.5\,\mathrm{c}$ (Li & Chevalier 1999). This is less even than the energy in gamma-rays from GRB 030329, unless the beaming angle is very small.

It is generally agreed that SN 1998bw was a very asymmetric explosion whose high velocities may not have characterized ejecta at all angles (e.g., Mazzali et al. 2001; Maeda et al. 2003), and the same seems likely to be true of SN 2003dh. Despite the fact that its radiation is not beamed like a GRB, an asymmetric supernova can have a quite different light curve from a spherical one of the same total energy. The higher velocities in one direction lead to the earlier escape of radiation and, in the case of a radioactive power source, a rapid decline in the deposition efficiency of gamma-rays. If the radioactivity itself is mixed out preferentially along one axis, the efficiency of gamma-deposition is also affected, leading to a more rapid rise and decline of the luminosity. On the other hand, the less rapidly moving matter ejected in other directions, can continue to contribute an extended tail on the light curve, powered by the remaining radioactivity.

In a pioneering study of light curves from asymmetric explosions, Höflich, Wheeler, & Wang (1999) modeled the light curve of SN 1998bw, but attempted to fit it into the general family of Type Ib/c supernovae. Their parameters were thus typical of these common events: ^{56}Ni mass (0.07 to $0.2\,\mathrm{M_\odot}$), ejected mass ($2\,\mathrm{M_\odot}$), and explosion energy (2×10^{51} erg). They, and Woosley, Eastman, & Schmidt (1999), championed the idea that asymmetrically exploded supernovae of the same energy may have different light curves. However, in light of SN 2003dh, neither went far enough.

Here we model the supernova as essentially two components - a slowly moving, high-mass

equatorial ejection and a lower mass polar ejection (see also Maeda et al. 2002, 2003). The juncture between these is almost discontinuous. A smooth transition would give too broad a light curve. The total mass of the progenitor, $\sim 10\,M_\odot$ of helium and heavy elements, the ^{56}Ni mass synthesized, $\sim 0.5\,M_\odot$, and the total explosion energy, $\sim 10^{52}$ erg, are all quite atypical for ordinary Type Ib/c supernovae.

2. EXPLOSION MODELS

A series of explosions was calculated for two Wolf-Rayet (WR) stars of final mass $8.39\,M_\odot$ and $15\,M_\odot$. Both models had an initial mass of $15\,M_\odot$ and an initial composition appropriate to the helium core of a star with 0.1 solar metallicity. Both models were started with a surface rotation rate corresponding to 30 % Keplerian at the equator. It was assumed, however, that the lower mass star was in a binary system and lost its hydrogen envelope to the companion star during the expansion phase after core hydrogen depletion (Case B mass transfer). This model continued to lose mass as a WR-star at a rate given by Braun (1997), reduced by $\sqrt{[\mathrm{Fe/Fe_\odot}]}$ (i.e., about a factor 3), and another factor 3 to account for clumping (Hamann & Koesterke 1998). The higher mass model, while lacking a hydrogen envelope, assumed no further mass loss. This was an artificial way to create two rapidly rotating WR-stars with a range of masses. For the given starting mass, the one evolved with mass loss is probably the more realistic.

In both calculations the effects of rotationally induced mixing were included (Heger, Langer, & Woosley 2000) throughout the evolution and both reached iron core collapse with sufficient angular momentum to form a Kerr black hole and an accretion disk. The adopted reaction rate for the ^{12}C$(\alpha,\gamma)^{16}$O reaction was 1.2 times that of Buchmann (1996). Both models had very fine surface zoning, down to less than 10^{21} g. The radii of the two stars at the time their cores collapsed were 8.1×10^{10} cm (with mass loss) and 8.8×10^{10} cm (without mass loss). Some other properties of the presupernova stars are given in Tables 1 and 2.

Explosions were simulated by placing a piston at the location of a large entropy jump, around $S/\mathrm{N_A k_B} = 4$, in the presupernova star when its peak infall velocity had reached about $1000\,\mathrm{km\,s^{-1}}$. Such a large change in entropy typically corresponds to a sudden decrease in density at the base of the oxygen-burning shell where mass bifurcations often develop in supernova models. The star outside this piston was first allowed to collapse to 500 km at one-fourth the free fall acceleration (inward movement of the piston). For the lower mass model, which only formed a small iron core (Table 2), the entropy jump and piston were at $1.462\,M_\odot$. For the higher mass model, a large collapsing low-entropy core formed (Table 2) and two piston locations were explored. One was located at $1.93\,M_\odot$, at the edge of the iron

core, the other at $2.75\,\mathrm{M_\odot}$ where the large entropy discontinuity occurred.

After the minimum radius was reached, the piston was moved outward supersonically, decelerating at constant fraction of gravitational acceleration until it coasted to a halt at $10,000\,\mathrm{km}$. The initial velocity and deceleration of the piston were adjusted to give the desired explosion energy. (The right piston acceleration has been determined using a modified regular FALSI algorithm.) This explosion energy here is defined as the final kinetic energy of the ejecta for an explosion into vacuum.

A wide range of kinetic energies was explored for these isotropic explosion (Table 3), including energies all the way up to $1.6 \times 10^{53}\,\mathrm{erg}$. This energy, half the binding energy of a typical neutron star, is far more than expected from any realistic neutrino-powered model, but, as we shall see, might be relevant for a small amount of mass ejected in a very asymmetric explosion in which the energy source is not neutrinos, but gravitational energy from accretion into a black hole. Nucleosynthesis was calculated as described in Weaver, Zimmerman, & Woosley (1978). An interesting result was the observation of a maximum mass of $^{56}\mathrm{Ni}$, regardless of explosion energy and depending only on the mass of the progenitor and depth of the piston.

A near constant mass, $0.2 \pm 0.05\,\mathrm{M_\odot}$ was synthesized in the $8.39\,\mathrm{M_\odot}$ models (Table 3). The near constancy of this upper bound is a consequence of the fast expansion and increasing entropy in the center of the ejecta that leads to freeze-out of $^4\mathrm{He}$ rather then $^{56}\mathrm{Ni}$ (Fig. 1). Eventually, turning up the energy only increases the ejection of α-particles, not of $^{56}\mathrm{Ni}$. Because the location of the piston cannot be much deeper in the $8.39\,\mathrm{M_\odot}$ model and because any other way of exploding the star, say by energy deposition rather than a piston, would give more photodisintegration, $\sim 0.2\,\mathrm{M_\odot}$ is the maximum $^{56}\mathrm{Ni}$ that can be synthesized in a spherically symmetric explosion of this star. A larger amount can be made in the $15\,\mathrm{M_\odot}$ star without mass loss because more mass sits closer to the piston. For a piston mass of $2.75\,\mathrm{M_\odot}$, the limiting mass of $^{56}\mathrm{Ni}$ was $\sim 0.6\,\mathrm{M_\odot}$. For a piston mass of $1.93\,\mathrm{M_\odot}$, the edge of the iron core, the limiting $^{56}\mathrm{Ni}$ mass was $1.1\,\mathrm{M_\odot}$ (Table 3). One might get still larger $^{56}\mathrm{Ni}$ masses by going to helium stars above $15\,\mathrm{M_\odot}$. However, this is the largest helium core one expects for stars near solar metallicity and larger mass cores will require even greater energies to expand rapidly enough to explain SN 2003dh.

That these limits are within a factor of two of the mass of $^{56}\mathrm{Ni}$ inferred (see below) for both SN 1998bw and SN 2003dh is interesting, but probably coincidental. The existence of an upper bound for shock powered models has interesting implications though (§ 5).

3. MODEL LIGHT CURVES

Light curves were calculated for all the explosion models using the KEPLER code as described, e.g., in Woosley, Eastman, & Schmidt (1999). Gamma-rays from ^{56}Ni and ^{56}Co decay were assumed to deposit locally. The gamma-ray opacity was $0.037\,\mathrm{cm^2\,g^{-1}}$. For the diffusing radiation, opacity was assumed to be predominantly electron scattering. The electron density was calculated by solving the Saha equation for the ionization structure at each point. Though calculated assuming a single-temperature, flux-limited diffusion, and a simple model for gamma-ray deposition, the curves should be qualitatively correct and suffice for present purposes.

Fig. 2 and the first frame of Fig. 3 show the light curves expected when the supernova experiences "moderate" mixing. Mixing was simulated by a running average of the composition within a region of mass, Δm, set here to $10\,\%$ of the final mass of the star. That is, the actual composition gradients were smoothed by averaging within a defined band of masses, and this band was itself moved out, zone by zone, from the piston to the surface. This procedure was repeated four times in each model. For the $8.38\,\mathrm{M_\odot}$ model with $1.25 \times 10^{51}\,\mathrm{erg}$ explosion energy, for example, this resulted in ^{56}Ni being mixed far enough out that it had $50\,\%$ of its central value (i.e., just above the piston) at about $3\,\mathrm{M_\odot}$ and $10\,\%$ at $5.5\,\mathrm{M_\odot}$ (as measured from the center of the collapsed remnant). The second panel of Fig. 3 shows similar light curves for the $8.35\,\mathrm{M_\odot}$ model when the composition is completely homogenized, i.e., made to be the same from center top surface. This might be the case if a vigorous asymmetric flow is responsible for exploding the star.

These are bolometric light curves, which properly should be compared only with luminosities integrated across the UVOIR bands. However, based upon our experience with SN 1998bw, we shall compare them with the observed V-band light curve of SN 2003dh (Hjorth et al. 2003). This shows the brightness rising to maximum at $10 - 13$ days (rest frame) and declining by 1 magnitude when the supernova was about 30 days old. The authors further estimate that the supernova was "slightly brighter" than SN 1998bw for which a peak luminosity $1.0 \times 10^{43}\,\mathrm{erg\,s^{-1}}$ (Woosley, Eastman, & Schmidt 1999) and ^{56}Ni mass 0.3 to $0.4\,\mathrm{M_\odot}$ has been estimated (Nakamura et al. 2001; Sollerman et al. 2002).

Though the ^{56}Ni mass ejected varies with kinetic energy and progenitor mass (Table 3), the supernova must have made a single value. Knowing the approximate luminosity we needed at peak, another series of light curves was calculated for which the yield of ^{56}Ni was normalized to $0.5\,\mathrm{M_\odot}$ in all the explosions, even for the low mass progenitor. This is a typical value for the very energetic explosions (Table 2), is close to the $0.3\,\mathrm{M_\odot}$ (Sollerman et al. 2002) to $0.4\,\mathrm{M_\odot}$ (Nakamura et al. 2001) of ^{56}Ni inferred for SN 1998bw, and is consistent with the observation that SN 2003dh was a little brighter than SN 1998bw (Hjorth et al.

2003). The fact that it is allowed to exceed the hydrodynamical limit derived in the previous section is justified because of the alternative way ^{56}Ni is made in the collapsar model (§ 4).

Such energetic models with so much ^{56}Ni are likely to be thoroughly mixed, more so than usual supernovae. Mixing proved necessary to obtain a good fit to the light curve of SN 1998bw, which accompanied GRB 980425 (Chugai 2000), and is favored by the rapid rise time in SN 2003dh. The third panel in Fig. 3 shows the light curves expected for the $8.39\,M_\odot$ models when the ejecta are thoroughly mixed and forced to contain a fiducial $0.5\,M_\odot$ of ^{56}Ni. This was accomplished by replacing as much of the material directly above the piston by pure ^{56}Ni as was needed to obtain the desired total ^{56}Ni mass. The replacement was done $100\,$s after the explosion when essentially all thermonuclear reactions have ceased, but before any mixing was applied.

Fig. 4 shows the terminal velocity for both models as a function of mass and Fig. 5 gives the velocity at the photosphere as a function of time and for the $8.38\,M_\odot$ model. In Fig. 4 only the intrinsically produced ^{56}Ni was considered, however, the energy release from ^{56}Ni decay has little effect on the expansion velocities, especially for the cases with high explosion energy. The fact that speeds as high as $\log\,(v/\mathrm{cm\,s^{-1}}) = 9.5$ were seen on SN 2003dh on day 10 (Hjorth et al. 2003) illustrates the need for at least some portion of the ejecta to have equivalent isotropic energies above $4\times10^{52}\,$erg. However, most of the models can give the milder requirement of $\log\,(v/\mathrm{cm\,s^{-1}}) \approx 9.0$ on day 30.

4. A "TWO-DIMENSIONAL" MODEL

Only the most energetic symmetric explosions, $E \gtrsim 10^{53}\,$erg, rise rapidly enough, make sufficient ^{56}Ni, and decay rapidly enough to resemble SN 2003dh. The velocities in these models are also consistent with what was seen (Fig. 5), but the energies strain credibility and even the most energetic model would not make a powerful gamma-ray burst. The correct model must be asymmetric.

Ideally, one would like to explore the coupled GRB-supernova explosion in two-dimensional code that couples radiation transport, gamma-ray deposition, and special relativistic hydrodynamics. Such calculations will surely be done, but as an expedient and for clarity in exposition, we consider here a simple, composite toy model rendered out of combinations of our one-dimensional models.

We rely here on experience with the collapsar model, especially MacFadyen & Woosley (1999) and Zhang, Woosley, & MacFadyen (2002). A black hole forms in the middle of the star and, after a few seconds while the polar accretion rate declines, launches relativistic jets

along both axes. These jets penetrate the star and ultimately make the GRB, but they do not, by themselves, make a supernova. The peak brightness of a Type I supernova of any subclass is measured by the ^{56}Ni that it ejects. Both the jets and the lateral shocks they launch make almost none. *Lacking additional sources of power, the supernova accompanying a collapsar-produced GRB would be weak and nearly invisible.*

That additional source of power is the wind off the accretion disk (MacFadyen & Woosley 1999; MacFadyen 2002; Pruet, Woosley, & Hoffman 2003). The mass ejected is of the same order as the mass accreted by the black hole, i.e., $\sim 1\,M_\odot$. It's energy is uncertain, but could easily be $\sim 10^{52}$ erg, that is the binding energy of a solar mass of material at the last stable orbit around a Kerr black hole times a few percent. A similar amount of energy is released by the reassembly of $0.5\,M_\odot$ of nucleons from the disk into bound nuclei. *Indeed the energy in this "wind" may considerably exceed the energy in the GRB-producing jets themselves.* Its composition is likely to be chiefly ^{56}Ni (Pruet, Woosley, & Hoffman 2003) mixed with the helium, oxygen, and other heavy elements that make up the star.

This wind drives a highly asymmetric explosion (MacFadyen & Woosley 1999). In fact, to first order, it blows two conical-shaped "wedges" out of the star, each along the rotational axis. In the case of SN 2003dh, because we saw the GRB, one of these inverted cones was directed straight at us. The equatorial regions are partly ejected, but partly fall into the hole, continuing to power the jet for some time after the initial explosion. The opening angle of the conical wedges is unknown, but certainly greater than the $\sim 5°$ opening of the GRB jet itself, yet probably small enough to contain only a fraction of the stellar mass. Here we will use $45°$ as an example. This implies that $1 - \cos\theta = 29\,\%$ of the star is ejected at very high velocity. Within this $45°$ we assume a Gaussian distribution of kinetic energies between 160×10^{51} erg and 40×10^{51} erg (Fig. 6) as a function of angle. We further assume a total production of $0.55\,M_\odot$ of ^{56}Ni, $90\,\%$ of which comes out in the high velocity (well-mixed) wedges, and $10\,\%$ of which stays behind in the low velocity ejecta.

The composite light curves were computed by assuming an explosion energy as a function of colatitude, θ:

$$E(\theta) = \begin{cases} 160 \times 10^{51} \text{ erg} \times \exp\left\{-0.5\,(\theta/\theta_1)^2\right\} & \text{for} \quad \theta \leq \pi/4 \\ 1.25 \times 10^{51} \text{ erg} & \text{for} \quad \theta > \pi/4 \end{cases} \tag{1}$$

where θ_1 is chosen such that $E(\pi/4) = 40 \times 10^{51}$ erg, i.e.,

$$\theta_1 = \frac{\pi}{4}\left(2\log\left(\frac{160 \times 10^{51} \text{ erg}}{40 \times 10^{51} \text{ erg}}\right)\right)^{-1/2}. \tag{2}$$

This was used to determine the flux as function of θ by interpolation in the grid of one-dimensional light curves. The one-dimensional models were calculated with an effective

mass of ^{56}Ni equal to $1.5\,\mathrm{M}_\odot$ (last panel of Fig. 3), i.e., a mass such that $29\,\%$ of it gave the actual ^{56}Ni mass in the high-velocity ejecta, $0.44\,\mathrm{M}_\odot$.

These contributions were then integrated over the projection of the sphere in the direction of the observer, along the pole (Fig. 7). Such a procedure does not take into account the "shadowing" effect of the fast moving polar ejecta on the slower equatorial ejecta. Owing to its fast expansion, the polar ejecta quickly become optically thin and the late-time light curve from the equatorial ejecta should not be significantly affected. We also do not take into account that the cone of high explosion energy may trap γ-rays less efficiently than a full sphere and thus cool down faster, or similarly, that the polar "hole" punched into the explosion by the jet could allow photons to escape faster in this direction, or that a larger fraction of the low-energy ejecta than corresponds to the projected surface area would become visible once the polar ejecta are optically thin. These truly two-dimensional effects may make the low-E part of the ejecta a little brighter early on and decline a bit faster at late times before the spherical model becomes optically thin.

The composite light curve corresponding to these assumptions is given in Fig. 8. During the first month, the luminosity is given entirely by the high-velocity, nickel-rich ejecta. Because of the high velocity and complete mixing the rise to maximum is very rapid. Because the material becomes thin and gamma-rays from radioactive decay escape, the decline from maximum is also fast. The decline of the light curve might be even faster than suggested by the composite model, because γ-rays can escape easier from a polar wedge than from a full sphere that has been used for modeling the light curves.

At late times though, the slower moving, nickel-poor ejecta dominate the light curve because gamma-ray deposition there remains highly efficient. For situations where the energy is due chiefly to radioactivity, this sort of light curve is distinctive signature of asymmetry. Models that expand slowly would not be so bright at peak and models that expand rapidly would not be so bright at late times. The amount of ^{56}Ni inferred from the peak brightness would be quite different from that inferred on the tail. Such seems to have been the case for SN 1998bw where a ^{56}Ni mass of $0.7\,\mathrm{M}_\odot$ was inferred for the peak (Iwamoto et al. 1998) and $0.24\,\mathrm{M}_\odot$ at late times (Nakamura et al. 2001).

5.   DISCUSSION

The optical light curve of the supernova that accompanies a typical GRB is unique in two ways. First, it must be disentangled from the "optical afterglow", which is dominated at early times by the relativistic GRB-producing jet interacting with the circum-source

medium. There will also be optical emission from slower moving, but still highly energetic supernova ejecta running into this medium. Continued, possibly time-variable output from the central engine also contributes at a declining rate to the afterglow at all wavelengths (Zhang, Woosley, & MacFadyen 2002). Whether one counts these afterglows as "supernova" or something else is largely a matter of taste. Supernova shock interactions have often been considered part of the light curve (Leibundgut 1994). They are probably the origin of variations in the early optical emission seen during the first few days of SN 2003dh (Willingale et al. 2003). Even with complete mixing, enormous explosion energy, and a large mass of ^{56}Ni, a supernova powered by radioactivity would not reach maximum light in two days.

Second, the supernova is grossly asymmetric. We have attempted to account for this by merging the results of several spherically symmetric models of various energies. Even so, large energies are required in the composite model, far above the GRB jet energy estimated by Frail et al. (2001). This energy must be provided by another source which, in the collapsar model, is the disk wind. Any attempt to model SN 2003dh without the formation of a black hole and disk must find a different way to produce the necessary ^{56}Ni and energy. The only other potential candidate at this time is a millisecond magnetar (Wheeler, Yi, Höflich, & Wang 2000). Provided the putative pulsar can survive accretion in a massive progenitor star long enough, it will need to deposit $\sim 10^{53}$ erg in ~ 1 s in order to make $\sim 0.5\,\mathrm{M_\odot}$ of ^{56}Ni in a high mass progenitor (making this much in a low mass model is impossible). The ^{56}Ni is required by the light curve and the high energy is required to make the star move fast enough to explain the rapid post-maximum decline of the supernova. The one-second time scale is set by the requirement that the ^{56}Ni be made by a shock that raises the temperature to greater than 5×10^9 K as is necessary to produce ^{56}Ni out of lighter elements. Concentrating the pulsar's energy in a smaller solid angle, as has been done here, will give a smaller ^{56}Ni mass no greater than $1.1\,\mathrm{M_\odot}$ times that solid angle (Table 3). In addition, the pulsar would need to focus some part of this energy into a very relativistic narrow jet (in order to make the GRB) at a time when the accretion rate is very high.

These potential difficulties lead us to favor the collapsar model. Based upon this model, in which the ^{56}Ni is provided by the disk wind in an explosion that is highly asymmetric we have developed a composite working model in which the total explosion energy is 26×10^{51} erg and the mass of ^{56}Ni is $0.55\,\mathrm{M_\odot}$. Further observations to test the predicted light curve (Fig. 8) are encouraged.

sity of Chicago.

REFERENCES

Braun, H. 1997, PhD thesis, Ludwig-Maximilians-Universität München

Buchmann, L. 1996, ApJ, 468, L127

Chugai, N. N. 2000, Astronomy Letters, 26, 797

Frail, D., Kulkarni, S. R., Sari, R., Djorgovski, S. G., Bloom, J. S., Galama, T. J. et al. 2001, ApJ, 562, L55

Galama, T. J., et al. 1998, Nature, 395, 670

Hamann, W.-R., Koesterke, L. 1998, A&A, 335, 1003

Heger, A., Langer, N., & Woosley, S. E. 2000, ApJ, 528, 368

Hjorth, J., Sollerman, J., Möller, P., Fynbo, J. P. U., Woosley, S. E., Kouveliotou, C., et al. 2003, Nature, 423, 847

Höflich, P., Wheeler, J. C., & Wang, L. 1999, ApJ, 521, 179

Iwamoto, K.Mazzali, P. A., Nomoto, K., Umeda, H., Nakamura, T., Patat, F., et al. 1998, Nature, 395, 672

Leibundgut, B. 1994, in *Circumstellar Media in Late Stages of Stellar Evolution*, eds. R.E.S. Clegg, I.R. Stevens & W.P.S. Meikle, (Cambridge University Press),100

Li, Z. & Chevalier, R. A. 1999, ApJ, 526, 716

MacFadyen, A. I., & Woosley, S. E. 1999, ApJ, 524, 262

MacFadyen, A. I. 2002, in *From Twilight to Highlight: The Physics of Supernovae*, eds. W. Hillebrandt & B. Leibundgut, ESO Astrophysics Symposia, p. 97.

Maeda, K., Nakamura, T., Nomoto, K., Mazzali, P. A., Patat, F., & Hachisu, I. 2002, ApJ, 565, 405

Maeda, K., Mazzali, P. A., Deng, J., Nomoto, K., Yoshii, Y., Tomita, H., & Kobayashi, Y. 2003, ApJ, 593, 931

Mazzali, P. A., Nomoto, K., Patat, F., & Maeda, K. 2001, ApJ, 559, 1047

Nakamura, T., Mazzali, P. A., Nomoto, K., & Iwamoto, K. 2001, ApJ, 550, 991

Pruet, J., Woosley, S. E., & Hoffman, R. D. 2003, ApJ, 586, 1254

Sollerman, J. et al. 2002, A&A, 386, 944

Stanek, K. Z., Matheson, T., Garnavich, P. M., Martini, P., Berlind, P., Caldwell, N., et al. 2003, ApJ, 591, L17

Weaver, T. A., Zimmerman, G. B., & Woosley, S. E. 1978, ApJ, 225, 1021

Wheeler, J. C., Yi, I., Höflich, P., & Wang, L. 2000, ApJ, 537, 810

Willingale, R., Osborne, J. P., O'Brian, P. T., Ward, M. J., Levan, A., & Page, R. L. 2003, submitted to MNRAS, astroph-0307561.

Woosley, S. E., Eastman, R. G., & Schmidt, B. P. 1999, ApJ, 516, 788

Zhang, W., Woosley, S. E., & MacFadyen, A. I. 2002, ApJ, in press, astro-ph/0207436

Table 1.   Properties[a] of the $15\,M_\odot$ progenitor model without mass loss

	m $(M_\odot)$	r (cm)	J (erg s)
iron core	1.95	2.58×10^8	1.23×10^{50}
Si core	2.61	4.99×10^8	2.35×10^{50}
Ne/Mg/O core	2.95	7.06×10^8	2.68×10^{50}
C/O core	8.56	5.16×10^9	2.24×10^{51}
star / He core	15.00	8.80×10^{10}	1.00×10^{52}

[a]Enclosed mass, m, radius, r, and enclosed angular momentum, J, of the progenitor model at core collapse or the outer boundaries of the indicated cores.

Table 2.   Properties of the $8.38\,\mathrm{M_\odot}$ progenitor model with mass loss

	m ($\mathrm{M_\odot}$)	r (cm)	J (erg s)
iron core	1.46	1.63×10^{8}	4.20×10^{49}
Si core	1.77	5.06×10^{8}	5.57×10^{49}
Ne/Mg/O core	1.88	6.77×10^{8}	5.96×10^{49}
C/O core	4.71	6.12×10^{9}	3.50×10^{50}
star / He core	8.38	8.09×10^{10}	1.38×10^{51}

Table 3.   Parameters of the Explosions

Mass ($M_\odot$)	8.38	15	15
Piston ($M_\odot$)	1.45	1.93	2.75
KE (10^{51} erg)		^{56}Ni ($M_\odot$)	
1.25	0.158	0.040[a]	0.024[a]
2.5	0.193	0.614[a]	0.225
5	0.229	0.707	0.254
10	0.244	0.815	0.303
20	0.230	0.938	0.377
40	0.189	1.045	0.487
80	0.168	1.083	0.583
160	0.170	0.955	0.625

[a]The ^{56}Ni mass is reduced by fallback after mild mixing. For the piston location at $1.93\,M_\odot$ the ^{56}Ni masses before fallback are $0.558\,M_\odot$ and $0.623\,M_\odot$; the total fallback mass is $6.889\,M_\odot$ and $0.050\,M_\odot$ (mass coordinates $8.819\,M_\odot$ and $1.980\,M_\odot$). For the piston location at $2.75\,M_\odot$ the ^{56}Ni mass without fallback is $0.192\,M_\odot$, the fallback mass is $5.580\,M_\odot$ (mass coordinate $8.330\,M_\odot$).
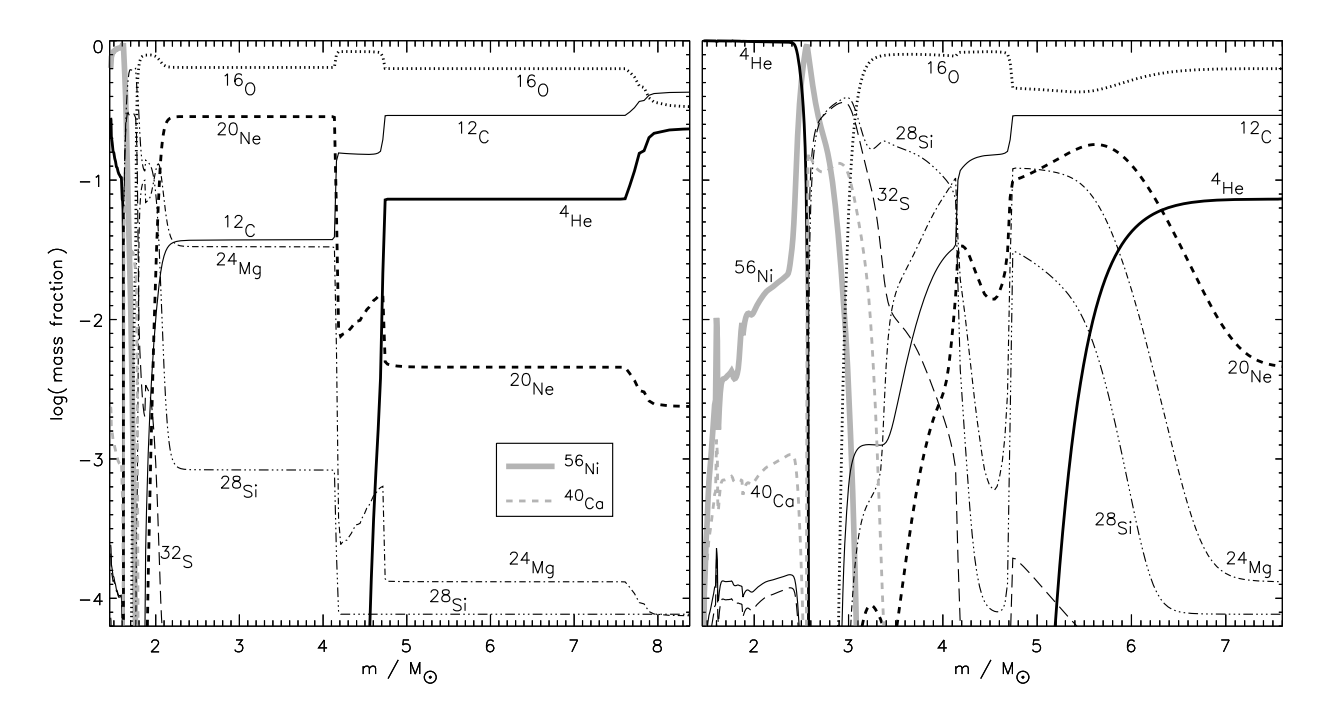
Fig. 1.— *Left:* Composition of the $8.38\,M_\odot$ star with 1.25×10^{51} erg explosion energy $100\,$s after core collapse, but prior to any mixing. *Right:* Same plot, but for the 160×10^{51} erg explosion. Note that $0.8\,M_\odot$ has been removed from the surface of this calculation because it exceeded $10^{10}\,$cm s^{-1} and posed problems for the non-relativistic hydro-code. Also note the large mass of photodisintegrated matter (^{4}He) in the inner regions near the mass cut. This limits the production of ^{56}Ni in the model.
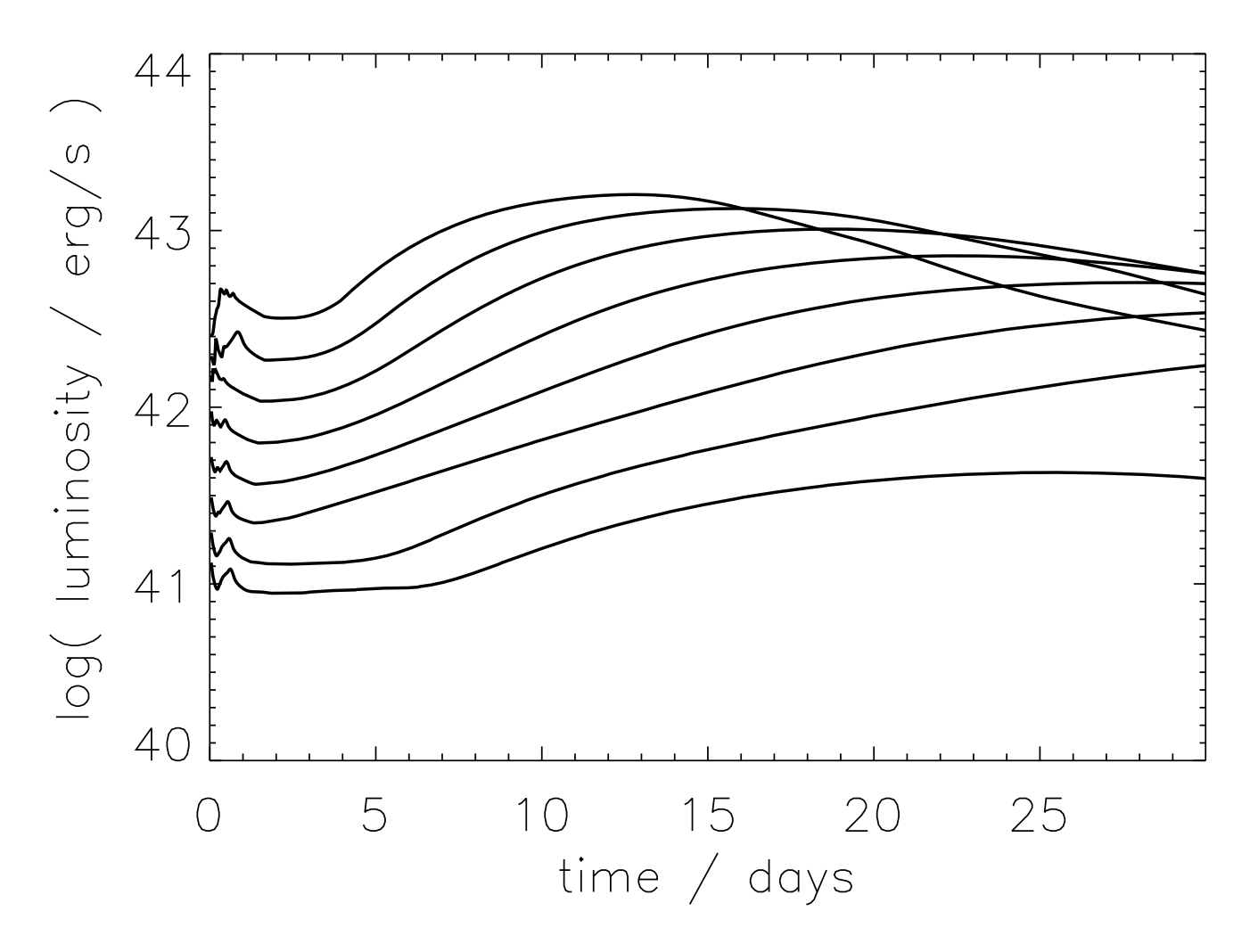
Fig. 2.— Light curves for "moderately" mixed models derived from the high mass progenitor $(15\,M_\odot)$ and the large piston mass $(2.75\,M_\odot)$. The explosions were calculated in spherical symmetry with kinetic energies at infinity of 160, 80, 40, 20, 10, 5, 2.5, and 1.25×10^{51} erg and the light curves include just the mass of ^{56}Ni produced explosively in the model (Table 3). Note the pre-maximum non-monotonic evolution of the most energetic models resulting from helium and heavy element recombination. For the most energetic explosions the initial rise for the first few hours is a numerical artifact of removing zones moving faster than $1/3\,c$.
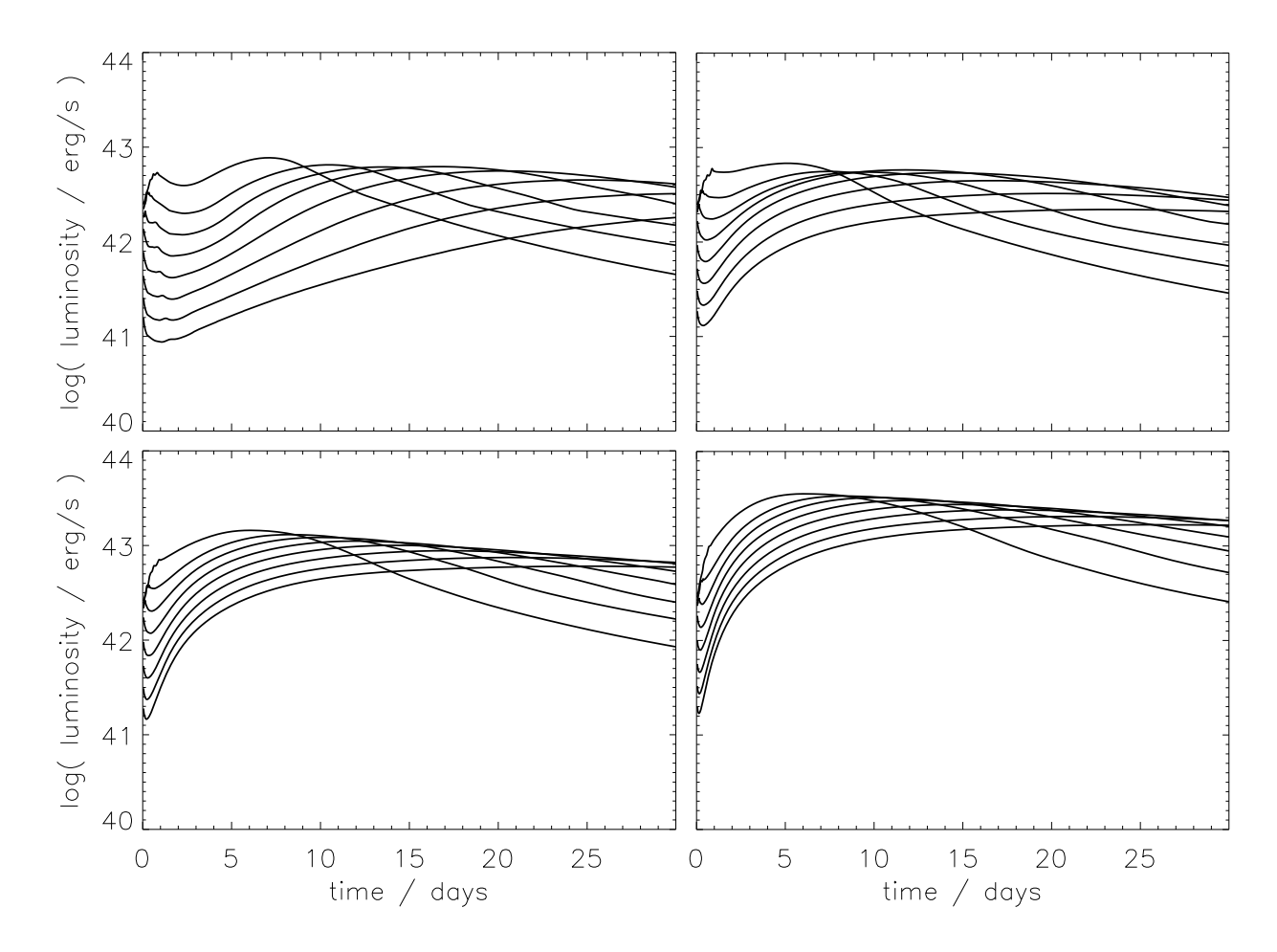
Fig. 3.— Light curves from the models for the low mass progenitor $(8.4 \, M_\odot)$. Calculated in spherical symmetry with kinetic energies at infinity of 160, 80, 40, 20, 10, 5, 2.5, and 1.25×10^{51} erg. See also Fig. 2. *Top Left:* Moderately mixed with the ^{56}Ni yields in Table 3. *Top Right:* Same models as top left, but completely mixed. *Bottom Left:* Completely mixed models with a normalized abundance of ^{56}Ni of $0.5 \, M_\odot$ in all cases. The peaks of the light curves are brighter owing to the increased mass of ^{56}Ni and the pre-maximum variability is less apparent. *Bottom Right:* Same mixed calculations normalized to a ^{56}Ni mass of $1.5 \, M_\odot$, as is appropriate for the high-velocity ejecta.
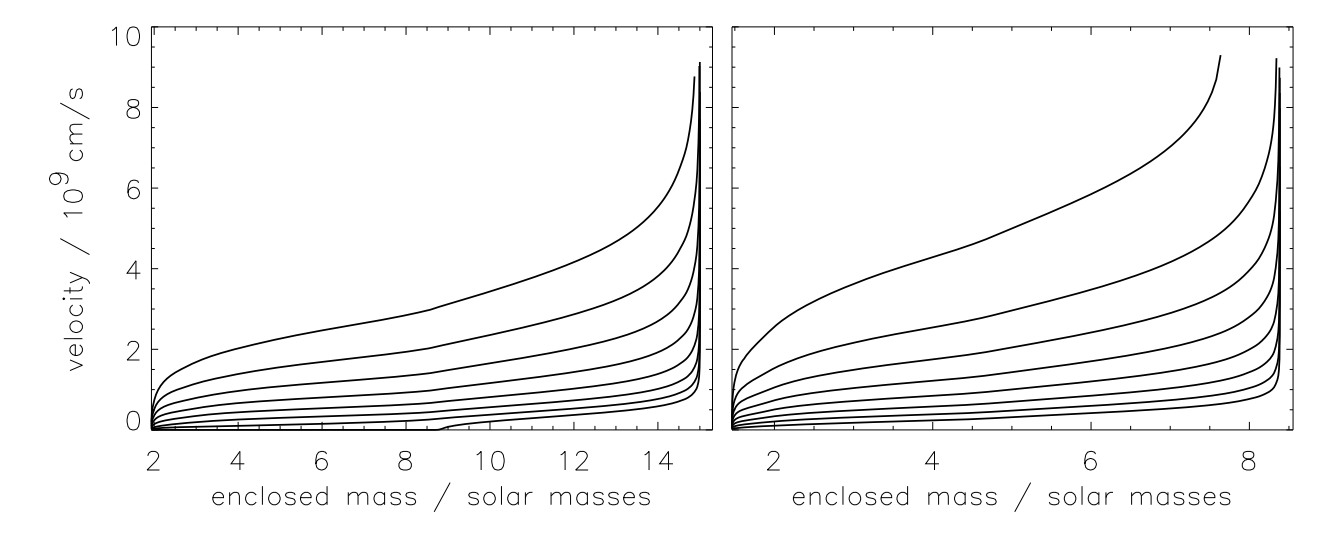
Fig. 4.— *Left:* Final velocity as a function of mass for a piston location of $1.93\,\mathrm{M_\odot}$ in the $15\,\mathrm{M_\odot}$ model. Moderate mixing and only the ^{56}Ni produced intrinsically by the explosion were used. Note fallback of $\sim 9\,\mathrm{M_\odot}$ for the lowest explosion energy. *Right:* Same plot, but for the $8.38\,\mathrm{M_\odot}$ model
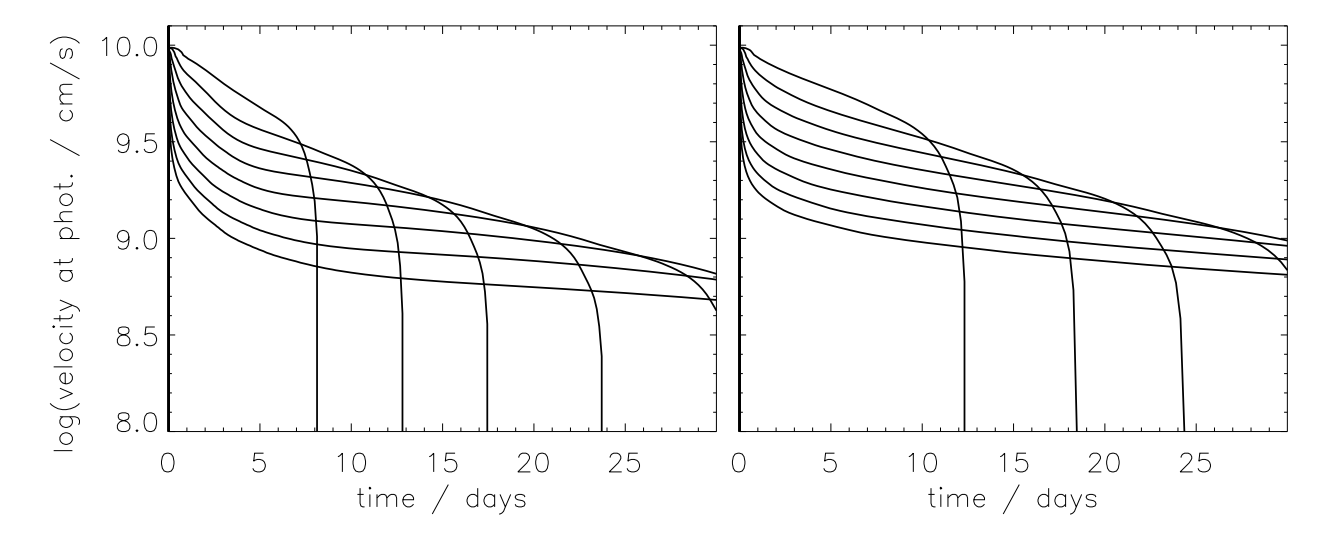
Fig. 5.— *Left:* Velocity at the photosphere for the 160, 80, 40, 20, 10, 5, 2.5, and 1.25×10^{51} erg explosions of the $8.38 \, \mathrm{M_\odot}$ star with moderate mixing and only its intrinsic ^{56}Ni production. Note that the velocity drops to zero and becomes undefined thereafter when the photosphere reaches the center of the ejecta. (A line of sight through the center would have an optical thickness of 4/3 at this point.) Also note that zones moving faster than $10^{10} \, \mathrm{cm \, s^{-1}}$ have been cut off from the calculations; this affects the velocity at the photosphere for about half a day for the most energetic explosion, and increasingly earlier times for lower energies. *Right:* Same plot, but for ejecta whose ^{56}Ni mass has been increased to $1.5 \, \mathrm{M_\odot}$ and the ejecta were "thoroughly mixed". Extra heating by the increased ^{56}Ni abundance at large radii maintains an extended photosphere longer.
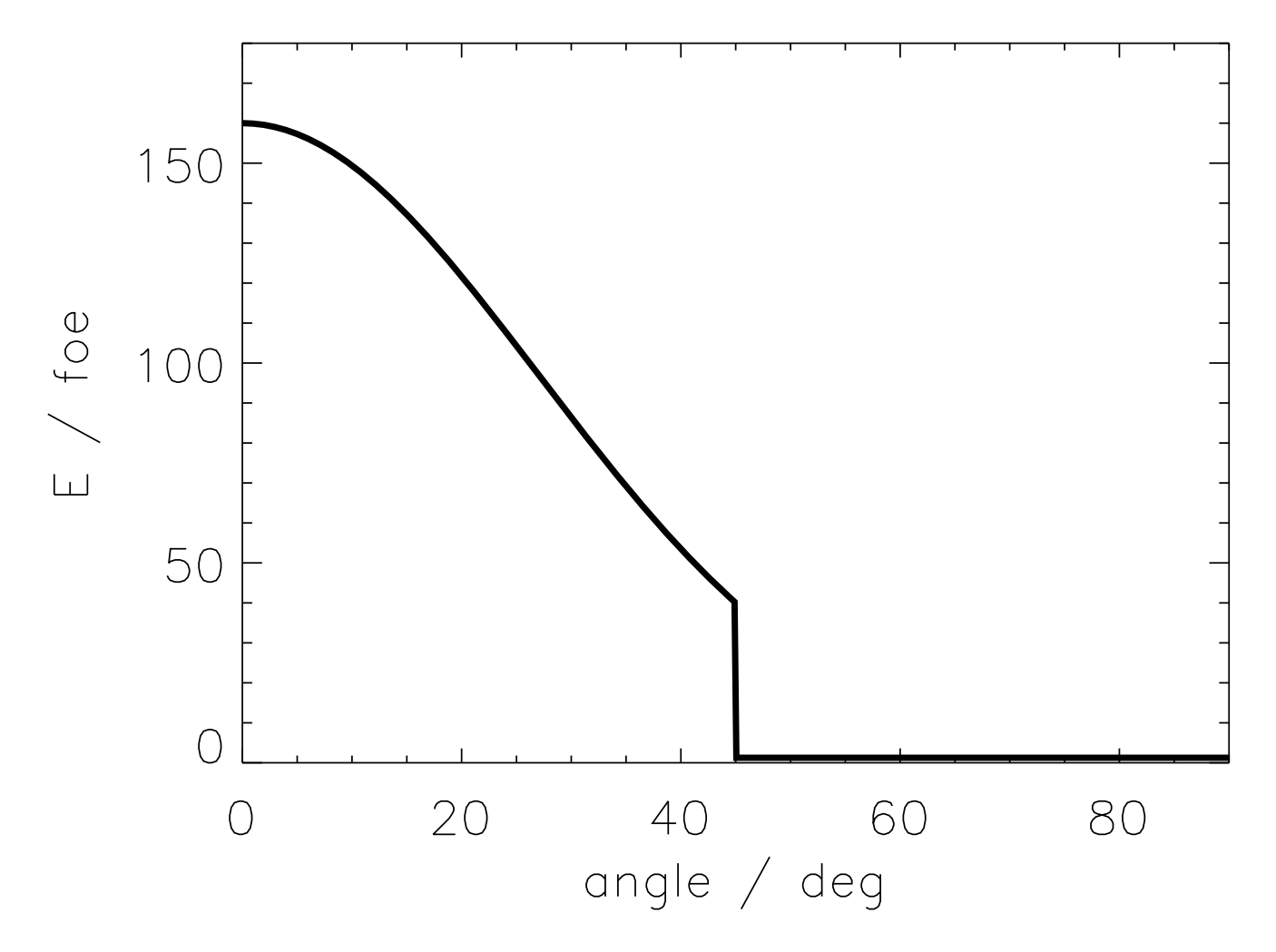
Fig. 6.— Contributions to the composite model. The figure gives the equivalent isotropic energy along a given angle as a function of angle. For angles less than 45° the energy varies from 160×10^{51} erg to 40×10^{51} erg and models normalized to $1.5\,M_{\odot}$ of ^{56}Ni were used, being "thorough" mixed. For angles greater than 45° the explosion energy is 1.25×10^{51} erg weak; only the intrinsic ^{56}Ni production (Table 2) and mild mixing was employed.
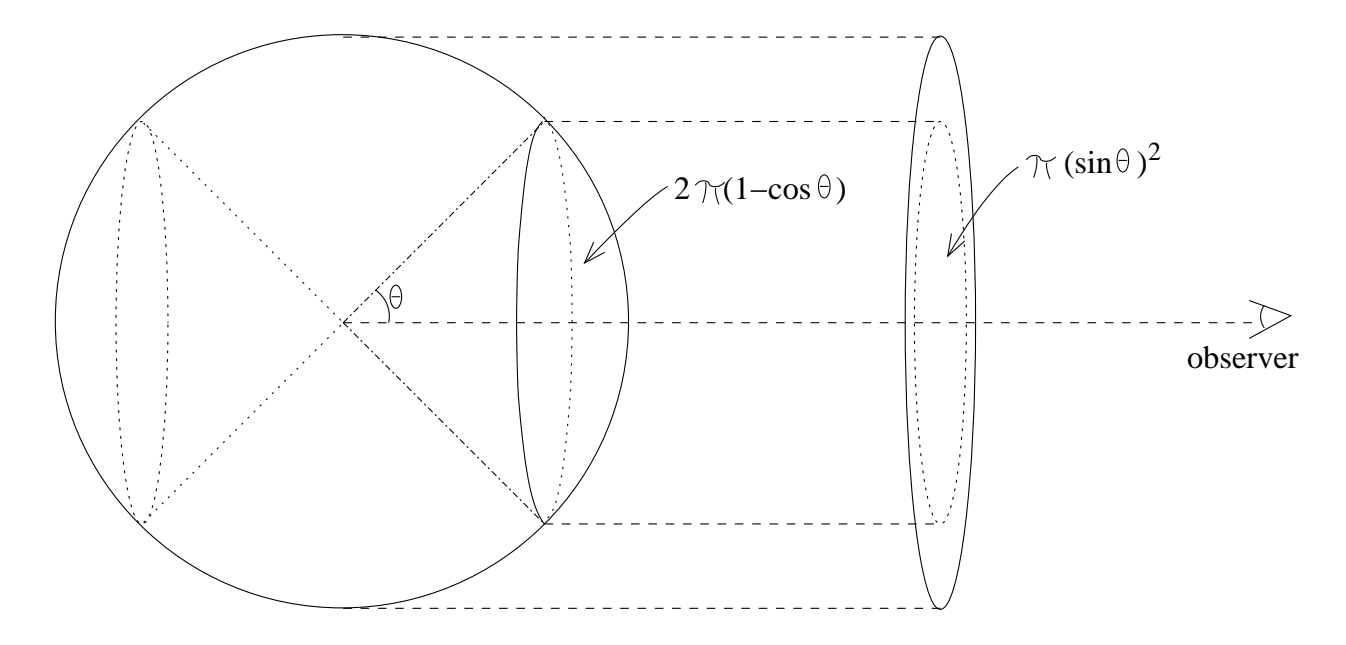
Fig. 7.— Decomposition of the light curve. Assuming, a (bipolar) jet of opening angle 2θ (e.g., $\theta = 45°$ as depicted above), each polar cap comprises a solid angle of $2\pi \left(1 - \cos \theta\right)$, i.e., the bipolar jet flows out at a fraction $1 - \cos \theta$ of the total solid angle of 4π. This means $1 - \cos \theta$ of the isotropic explosion contributes to such an explosion and its energy. However, an observer looking along the axis of the jet sees the projected surface area $\pi \left(\sin \theta\right)^2$ out of 2π for the full circle, the full projected sphere, i.e., a fraction $\sin^2 \theta$ of the isotropic light curves contributes to apparent light curve for a such positioned observer. Note that for $0° < \theta < 90°$: $\sin^2 \theta > 1 - \cos \theta$, i.e., the observer along the axis is favored to see an apparently brighter light curve than would correspond to the total energy of a composed light curve (assuming the explosion is stronger in polar direction than in equatorial direction). This is because material at high colatitude, θ, appears under a high inclination angle.
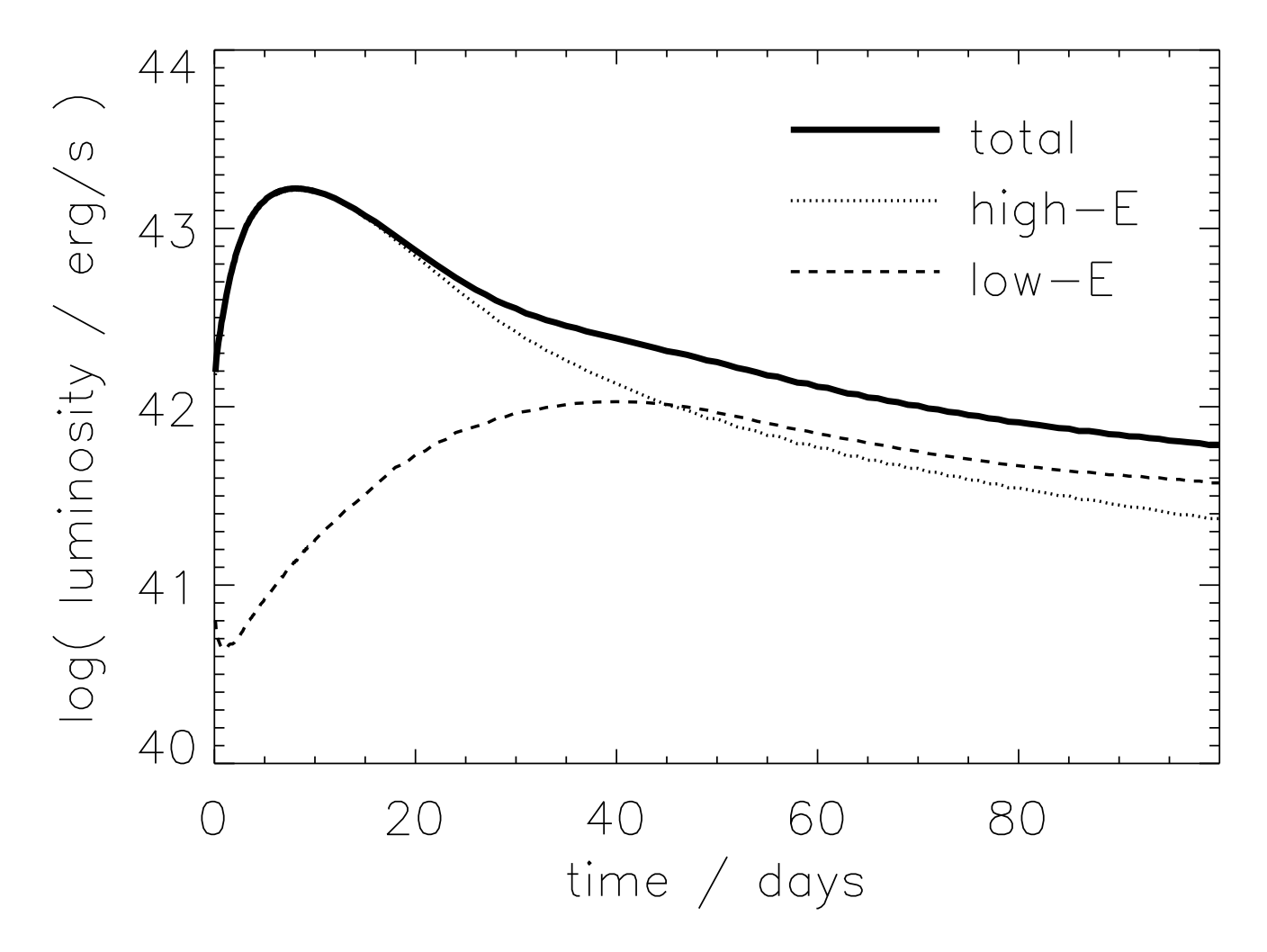
Fig. 8.— Composite light curve resulting from a combination of well-mixed models (Fig. 3) having a distribution of kinetic energies as given in Fig. 6. For polar angles less than 45° the three highest energy models in Fig. 3 were employed which each have an effective ^{56}Ni mass of $1.5\,\mathrm{M_\odot}$. Together, with appropriate angular weighting (see text), these give the curve labeled "high-E". For angles greater than 45° the model with energy 1.25×10^{51} erg in Fig. 3 was used. The ^{56}Ni mass in this component was left at $0.15\,\mathrm{M_\odot}$. This curve, with appropriate weighting, is labeled "low-E". The dark solid line is the total. The total energy in the composite is 26×10^{51} erg and the total mass of ^{56}Ni is $0.55\,\mathrm{M_\odot}$.